CHEMISTRY OF MATERIALS

pubs.acs.org/cm

Article

Dysprosium Incorporation for Phase Stabilization of Atomic-Layer-Deposited HfO_2 Thin Films

Yujin Lee, Kangsik Kim, Zonghoon Lee, Hong-Sub Lee, Han-Bo-Ram Lee, Woo-Hee Kim,* Il-Kwon Oh,* and Hyungjun Kim*

Cite This: *Chem. Mater.* 2023, 35, 2312−2320

Read Online

ACCESS | Metrics & More | Article Recommendations | Supporting Information

ABSTRACT: The relatively low thermal stability of HfO_2 films severely affects the performance of semiconductor devices. For instance, the low crystallization temperature of HfO_2 (~500 °C) leads to the formation of grain boundaries, which increases the leakage current. In this study, Dy incorporation leads to the phase transformation of HfO_2 films from various directional planes to a main m(−111) plane by the crystallographic stabilization of HfO_2 films, increasing the size of grains. Dy-doped HfO_2 thin films with modulated doping content, prepared by plasma-enhanced atomic layer deposition (PE-ALD), are characterized by analysis of their chemical composition combined with electron microscopy and synchrotron X-ray techniques. The transformation from m(110), m(−111), m(111), m(020), and m(120) to a main m(−111) plane is observed through X-ray diffraction, which indicates that Dy plays a role for the phase stabilization of HfO_2 films. The atomic-scale images of the cross section and top view obtained using an electron microscope demonstrate that the in-plane average grain size is increased by approximately 4 times due to Dy incorporation compared with that of single HfO_2 films. The reduction in the area of the grain boundary of HfO_2 due to Dy incorporation decreases the leakage current density of HfO_2 by 1000 times and increased the breakdown strength. This result can aid future electronics by determining the effect of a dopant on the crystallographic structure of host thin-film materials.

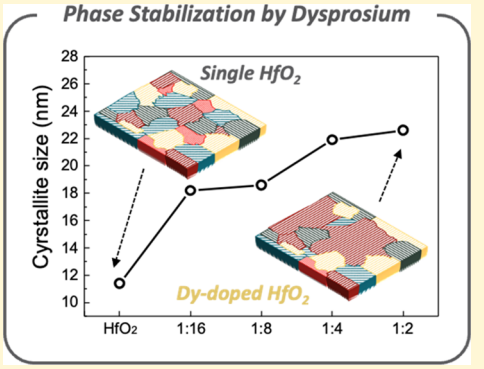

1. INTRODUCTION

It is crucial to develop dielectrics with high permittivity and decrease the leakage current caused by direct tunneling to enable the continuous scaling of the effective thickness of dielectrics in semiconductor devices.[1−3] High-*k* materials such as HfO_2, La_2O_3, Ce_2O_3, Y_2O_3, and Dy_2O_3 have been considered as possible alternative gate dielectrics for future technologies.[4−7] HfO_2 has attracted significant attention owing to its high conduction and valence band offsets to Si (<1 eV), moderately high dielectric constant (19−25), and good thermal stability with Si.[8−10] Additionally, Hf-based dielectrics such as HfO_2 or $Hf_xSi_{1-x}O_2$ in conjunction with metal gate electrodes have been practically employed in sub-30 nm CMOS technology nodes.[11]

However, the further improvement of HfO_2 performance is required for future electronics. For example, the low crystallization temperature (approximately 500 °C) of HfO_2 films degrades its performance in CMOS devices because the grain boundaries provide a conductive path resulting in leakage current across the gate stack, which increases the power consumption in circuits.[12] Several elements such as Si,[8] Al,[13] N,[14] Ta,,[15] La,[16] and Dy[5,7] have been doped into HfO_2 films to improve the crystallization temperature. Among them, rare earth metal oxides are of considerable interest for logic and memory device applications by virtue of their high permittivity values, large band gaps, and thermodynamic stability when deposited directly on silicon.[5,7,14] However, their hygroscopic nature and ability to absorb CO_2 from air lead to the retention of moisture and subsequent reaction with water imposes challenges in the integration of La_2O_3.[17] Dy_2O_3 has been reported to be the least reactive with water and thermodynamically stable with Si.[18]

Previous studies have discussed the V_{fb}/V_{th} shift and reduction of leakage currents through magnetron-sputtered Dy doping into HfO_2.[5,7,19] The higher packing density of DyHfO alloy than that of HfO_2 and lower electronegativity of Dy than that of Hf significantly suppresses the leakage current by reducing the oxygen vacancies in Dy-doped HfO_2 dielectrics.[7,19] Further studies have demonstrated that decreasing the O-vacancy reduces the density of the trap and, consequently, the tunneling currents.[20] In other words,

Received: September 17, 2022
Revised: February 28, 2023
Published: March 16, 2023

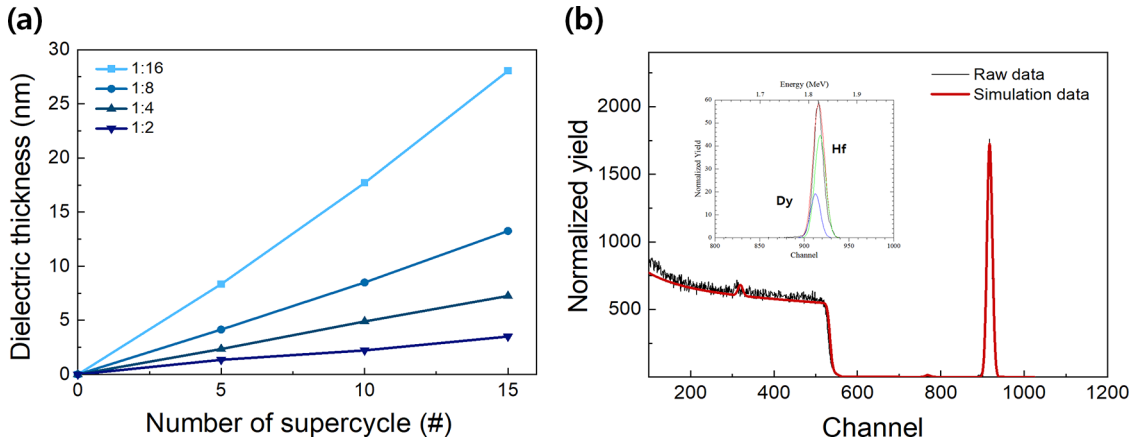

Figure 1. (a) Dielectric thickness as a function of the number of supercycles with varying ALD cycle ratio (Dy_2O_3/HfO_2) and (b) RBS analysis results of 1:2 Dy-doped HfO_2 film.

previous studies inferred the reduction of oxygen vacancies through electrical characteristics. On the other hand, it is known that the grain boundaries in thin films are mainly composed of oxygen vacancies. For this reason, we explain the correlation between Dy-doping and the chemical and structural modification caused in HfO_2-based dielectrics. Furthermore, various factors, such as band structure and film density, can also affect the leakage current density of gate dielectrics in addition to oxygen vacancies and film crystallinity. Therefore, the effects of Dy-doping into HfO_2 films were systematically investigated in this study, focusing on the comprehensive change in chemical and structural properties caused by Dy incorporation.

Meanwhile, previous reports on sputtered Dy-doped HfO_2 films were limited by effectively doping Dy into the HfO_2 films in terms of modulation of Dy doping concentration.[5,7] Atomic layer deposition (ALD) is advantageous compared to other deposition methods as it produces high-quality, ultrathin, uniform, and better-conformality gate dielectric films with low impurity contamination at low growth temperatures because the growth mechanism is based on a self-limited surface reaction.[11] Moreover, the ALD supercycle process consists of one cycle of dopant material followed by multiple repetitions of HfO_2 cycles that can effectively modulate the doping concentration of DyHfO alloy. Additionally, the application of plasma-enhanced ALD (PE-ALD) facilitates the chemical reactions between radicals with high reactivity, which allows deposition at significantly lower temperatures than that of conventional thermal ALD. Moreover, the presence of ions and electrons in the plasma produces high-quality film properties, which enhances the device performance.[21−23]

In this study, the growth characteristics and film properties of PE-ALD Dy_2O_3 films deposited using bis-isopropylcyclopentadienyl-di-isopropylacetamidinate-dysprosium ($Dy(iPrCp)_2(N\text{-}iPr\text{-}amd)$) precursor and O_2 plasma were investigated. The structural and electrical properties of Dy-doped HfO_2 films with different Dy/(Dy + Hf) compositions were investigated using a series of systematic physical and chemical characterization techniques. The phase transformation of Dy-doped HfO_2 films was studied based on their Dy content, which was explored in correlation with the crystallographic phase and grain size. Moreover, the electrical properties of Dy-doped HfO_2 films such as leakage current density and breakdown strength were investigated.

2. EXPERIMENTAL DETAILS

A commercial 8-inch ALD reactor (NCD Co., Lucida M100-PL) was used with a showerhead to ensure optimum uniformity. Bis-(isopropylcyclopentadienyl) diisopropylacetamidinate dysprosium ($Dy(iPrCp)_2(N\text{-}iPr\text{-}amd)$) and hafnium tetrachloride ($HfCl_4$) precursors contained in stainless-steel bubblers were used to perform the ALD of Dy_2O_3 and HfO_2, respectively. They were evaporated at 130 and 170 °C, respectively, to obtain a sufficiently high vapor pressure. The temperature of the delivery lines was maintained at 15 °C higher than that of the bubblers to prevent the condensation of precursor molecules. The precursor vapors were carried into a reactor chamber using Ar carrier gas at a flow rate of 50 sccm, which was controlled by a mass flow controller (MFC). Ar gas with the same flow rate was used to purge excess gas molecules and byproducts between each precursor and reactant exposure step. A flow rate of 200 sccm of oxygen gas was maintained using an MFC during PE-ALD and the frequency was set at 13.56 MHz, which provided a power level of 300 W. The PE-ALD supercycle process was performed for Dy-doping into HfO_2, which consisted of one PE-ALD Dy_2O_3 cycle followed by n repetitions of PE-ALD HfO_2 cycles. This enabled the modulation of Dy/(Dy+Hf) compositions in PE-ALD Dy-doped HfO_2 films. The substrate temperature was maintained at 180 °C during the PE-ALD process. The process timings (for the sequence composed of precursor exposure, purge, reactant exposure, and purge) were 2−5−1−5 s and 1.5−5−1−5 s for PE-ALD Dy_2O_3 and HfO_2, respectively.

Metal−oxide semiconductor (MOS) capacitors were fabricated to evaluate the electrical properties of PE-ALD dielectrics. PE-ALD Dy-doped HfO_2 films with various cycle ratios of Dy:Hf = 1:n (n = 16, 8, 4, and 2), and Dy_2O_3, and HfO_2 films were deposited on p-type Si substrates (001), which were cleaned at 70 °C for 10 min in RCA solution (1:1:5(v/v/v) $NH_4OH/H_2O_2/H_2O$). Subsequently, the films were dipped in a buffered oxide etchant solution for 30 s to remove native oxides. Post-deposition annealing (PDA) was performed after oxide deposition using a rapid thermal annealing (RTA, SNTEK Co.,) system at 600 °C in a nitrogen environment for 10 min to reduce trap charge densities. Finally, Ru was deposited as a metal gate through a patterned shadow mask by sputtering (SNTEK Co.,).

The thickness and refractive index of the deposited films were measured using a spectroscopic ellipsometer (Ellipso Technology, Elli-SE-F). The microstructure of the films was analyzed by using the in-plane mode of grazing-incidence X-ray diffraction (GIXRD, Rigaku, ATX-G). Additionally, the atomic-scale microstructure was observed using transmission electron microscopy (TEM, JEM 2100) at an accelerating voltage of 200 kV. The specimens for TEM observations were prepared by tripod polishing and low-angle ion milling using 1050 TEM mill (E.A. Fischione Instruments) focused Ar^+ ion thinning for cross-sectional and plan-view observations. The chemical composition, impurity level, and elemental quantification were

https://doi.org/10.1021/acs.chemmater.2c02862
Chem. Mater. 2023, 35, 2312−2320

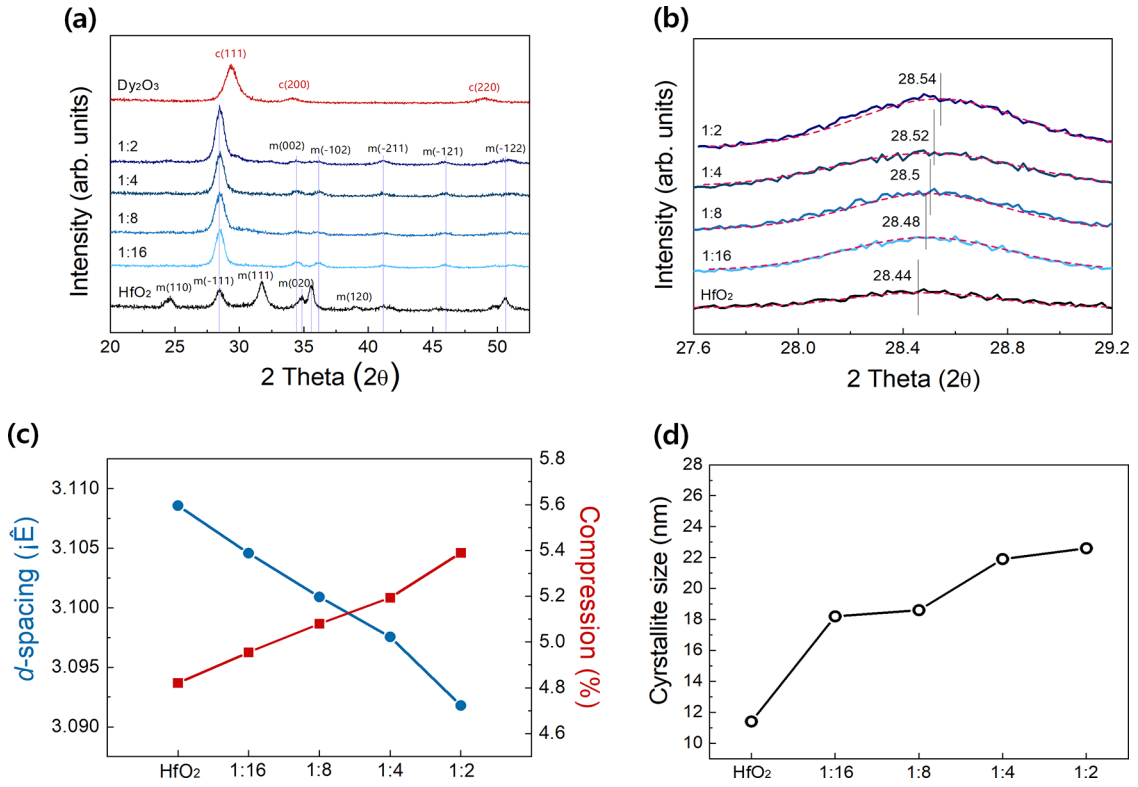

Figure 2. (a) XRD patterns of single Dy_2O_3, HfO_2, and Dy-doped HfO_2 films and (b) XRD patterns around the m(−111) plane, (c) *d*-spacing ($d_{(-111)}$) and compressive stress, and (d) crystallite size of single HfO_2 and Dy-doped HFO_2 films.

analyzed by Rutherford backscattering spectroscopy (RBS, NES). The band structure of the PE-ALD Dy-doped HfO_2 films was investigated by photoemission spectroscopy (PES) measured in the 4D beamline of the Pohang Accelerator Laboratory (PLS). The valence band spectrum was obtained using 90 eV radiation. An Au foil was used as the reference material for energy calibration. Electrical properties based on capacitance−voltage ($C-V$) and current−voltage ($I-V$) characteristics were measured using a Keithley 590 $C-V$ analyzer and Agilent 4155C semiconductor parameter analyzer, respectively.

3. RESULTS AND DISCUSSION

PE-ALD HfO_2 and Dy_2O_3 processes were used to deposit Dy-doped HfO_2 films with various ALD cycle ratios (Dy_2O_3/HfO_2) to systematically examine the effects of Dy doping into the HfO_2 gate dielectric. Herein, the number of ALD HfO_2 cycles per supercycle (n) was modulated in the range of n = 2−16 (Dy_2O_3:HfO_2 = 1:n with n = 2, 4, 8, and 16). The thickness per total number of growth cycles is plotted in Figure 1a for Dy-doped HfO_2 films with different ALD cycle ratios. Linear growth characteristics were observed regardless of the Dy composition. An increase in the slope was observed when the HfO_2 cycle ratio was gradually increased, which was attributed to significantly lower growth per cycle of ALD Dy_2O_3 (~0.3 Å/cycle) compared with that of ALD HfO_2 (~1.3 Å/cycle).[24,25] The change in the film thickness with an increase in the HfO_2 cycle ratio indicated that ALD enabled fine thickness control of Dy-doped HfO_2 films. In addition, a Dy-doped HfO_2 film was selected to accurately measure the atomic composition in ternary films by RBS. Figure 1b shows that the Dy/(Dy + Hf) ratio for the 1:2 sample was approximately 0.569, wherein the composition of Dy-doped HfO_2 films was $Dy_{0.45}Hf_{0.34}O_2Cl_{0.019}$ at an atom density of 8.0 × 10^{16} atoms/cm^2.[26,27]

Figure 2a depicts the XRD patterns of 20 nm thick HfO_2, Dy_2O_3, and 1:2, 1:4, 1:8, and 1:16 Dy-doped HfO_2 films annealed at 600 °C. The HfO_2 film exhibited a polycrystalline structure with monoclinic phases with (110), (−111), (111), and (−122) reflections, whereas the Dy_2O_3 film exhibited a polycrystalline structure with cubic phases with (111), (200), and (220), which were consistent with that of previous studies.[26,27] In the case of the 1:16 Dy-doped HfO_2 film, the polycrystalline structure of HfO_2 was changed to the preferred orientation of the monoclinic (−111) phase, while the intensity of monoclinic peaks including in (110), (111), (020), (120), and (−122) was significantly reduced. As the Dy concentration is increased to 1:2, a similar crystalline structure was observed as shown in Figure 2a with increased intensity. Additionally, the cubic phase of Dy_2O_3 was not observed in Dy-doped HfO_2 films, which indicated that Dy doping led to a well-organized structure without phase separation between HfO_2 and Dy_2O_3. The (−111) plane exhibits the lowest surface energy in monoclinic HfO_2.[28] Therefore, the growth of monoclinic HfO_2 films with crystallites in preferred (−111) texturing is thermodynamically favorable in comparison with that of other directional planes. Cisneros-Morales and Aita reported a similar result for sputtered HfO_2 films grown on silica substrates that exhibited preferential (−111) orientation.[29] Plasma may also influence this change in crystallinity due to film densification or ion bombardment. However, considering that the total plasma exposure time used in the process for obtaining the same thickness is similar, it is assumed that the plasma effect on the change in crystallinity would be insignificant.

High-resolution scans of the (−111) peak are shown in Figure 2b. The gradual shift to a higher diffraction angle with an increase in the Dy content in HfO_2 films can be observed.

https://doi.org/10.1021/acs.chemmater.2c02862
Chem. Mater. 2023, 35, 2312−2320

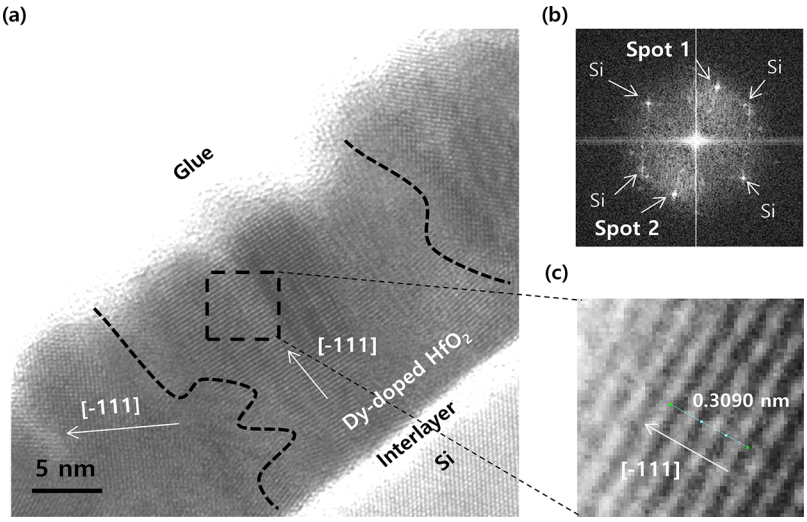

Figure 3. (a) Cross-sectional TEM image, (b) TEM-FFT diffraction pattern, and (c) TEM images of the m(−111) plane of Dy-doped HfO_2 film with the 1:2 ALD cycle ratio.

This was due to the changes in the interatomic *d*-spacing and crystallite size(D). The *d*-spacing ($d_{(-111)}$) versus Dy content plots are shown in Figure 2c. It should be noted that the $d_{(-111)}$ decreased with an increase in the Dy content. The *d*-spacing variation for (−111) planes dependent on the Dy contents can be used to obtain quantitative information about the lattice strain in the doped HfO_2 films. Therefore, a strain factor called compression (Γ), which is derived from the lattice mismatch, was calculated using the following formula in Figure 2c.[29]

$$\Gamma = \frac{d_{(100)\mathrm{Si}} - d_{(-111)\mathrm{sample}}}{d_{(-111)\mathrm{sample}}} \times 100\ (\%)$$

It can be observed that the Γ (%) increased with an increase in the Dy content due to the incorporation of Dy atoms in the HfO_2 film, which indicated an inverse relationship with *d*-spacing. Since the covalent radius of Dy atom (192 pm) is larger than that of Hf (175 pm), the incorporation of Dy atoms in HfO_2 films can cause voids or disordering of the lattice in HfO_2, which can generate compressive stress in HfO_2 films. This compressive stress can considerably affect the orientation of the crystal face,[30] so the incorporation of Dy atoms enables crystalline formation in the (−111) direction in this work. In addition, the D values calculated from the full width at half-maximum (FWHM) as a function of Dy content are plotted in Figure 2d. It should be noted that the value of D increased with an increase in the Dy content in HfO_2 films. These results demonstrated that the Dy atoms enabled the phase transformation to the main directional plane and increased the crystallite size. According to the previous report, as the crystallite size of a directional plane increases, the free energy decreases.[31] In other words, as the Dy concentration increases, the crystallite size of the most stable (−111) plane among the monoclinic planes of HfO_2 increases, indicating that Dy plays a role in phase stabilization in HfO_2 thin film.

The microstructure of the 10 nm thick Dy-doped HfO_2 film with a 1:2 cycle ratio was analyzed using the cross-sectional TEM image shown in Figure 3a to further investigate the crystallinity. In general, when depositing the thin film on the Si substrate using ALD, the 1−2 nm thick HfO_2 film near the interface has an amorphous phase. Then, with increasing the thickness of the thin film, the crystallinity could be affected due to changes in the stress inside the thin film as the thickness increases.[32] Such internal stress could exist in the 1−2 nm thick HfO_2 film near the interface, but crystals may not be formed due to the influence of the substrate. In this case, the vicinity of the interface with Si remains amorphous and gradually forms a crystal structure as the thickness increases.[33] However, judging from our TEM results, the formation of the crystalline phase is observed even at the very first layer on the interlayer. Considering that the crystallization of HfO_2 starts at about 500 °C or higher and that our process temperature is 180 °C, the crystalline formation at the interface might be not due to the annealing effect.[34] Therefore, it is presumed that the incorporated Dy atom would play a role in changing the crystallinity in the HfO_2 lattice structure so that the thin film could show crystallinity from the beginning of growth. The result of the fast Fourier transformation (FFT) for the entire region in the TEM image is shown in Figure 3b. Six reflections were observed at spots 1 and 2 and the Si (001) peaks. Herein, spots 1 and 2 represent the highest peak intensities, which correspond to the monoclinic (−111) plane of HfO_2 in the XRD data. Additionally, it can be confirmed from the intensity profile of the cyan-colored-line denoted along the [−111] direction that the lattice constant of the Dy-doped HfO_2 was approximately 0.309 nm, which indicated a monoclinic (−111) phase as shown in Figure 3c.

Single HfO_2 and Dy-doped HfO_2 films (1:2 ratio) were analyzed using plan-view TEM to evaluate the average grain size. The images are presented in Figure 4a,b, wherein the insets represent magnified images. The Dy-doped HfO_2 film exhibited an increased grain size compared with that of single HfO_2 films. The estimated grain diameter of the single HfO_2 film was approximately 50 nm, which was three times smaller than that of the 1:2 Dy-doped HfO_2 films as shown in the insets of Figures 4a and 4b. However, these values are larger than that of the crystallite size obtained through XRD as shown in Figure 2d. According to a previous study, this phenomenon is related to dislocation. In the case of a dislocation with a small orientation difference, XRD recognizes it as two different regions. Conversely, TEM recognizes this difference as a large grain rather than a grain boundary.[35] Therefore, the results would exhibit different values in XRD and TEM.

https://doi.org/10.1021/acs.chemmater.2c02862
Chem. Mater. 2023, 35, 2312−2320

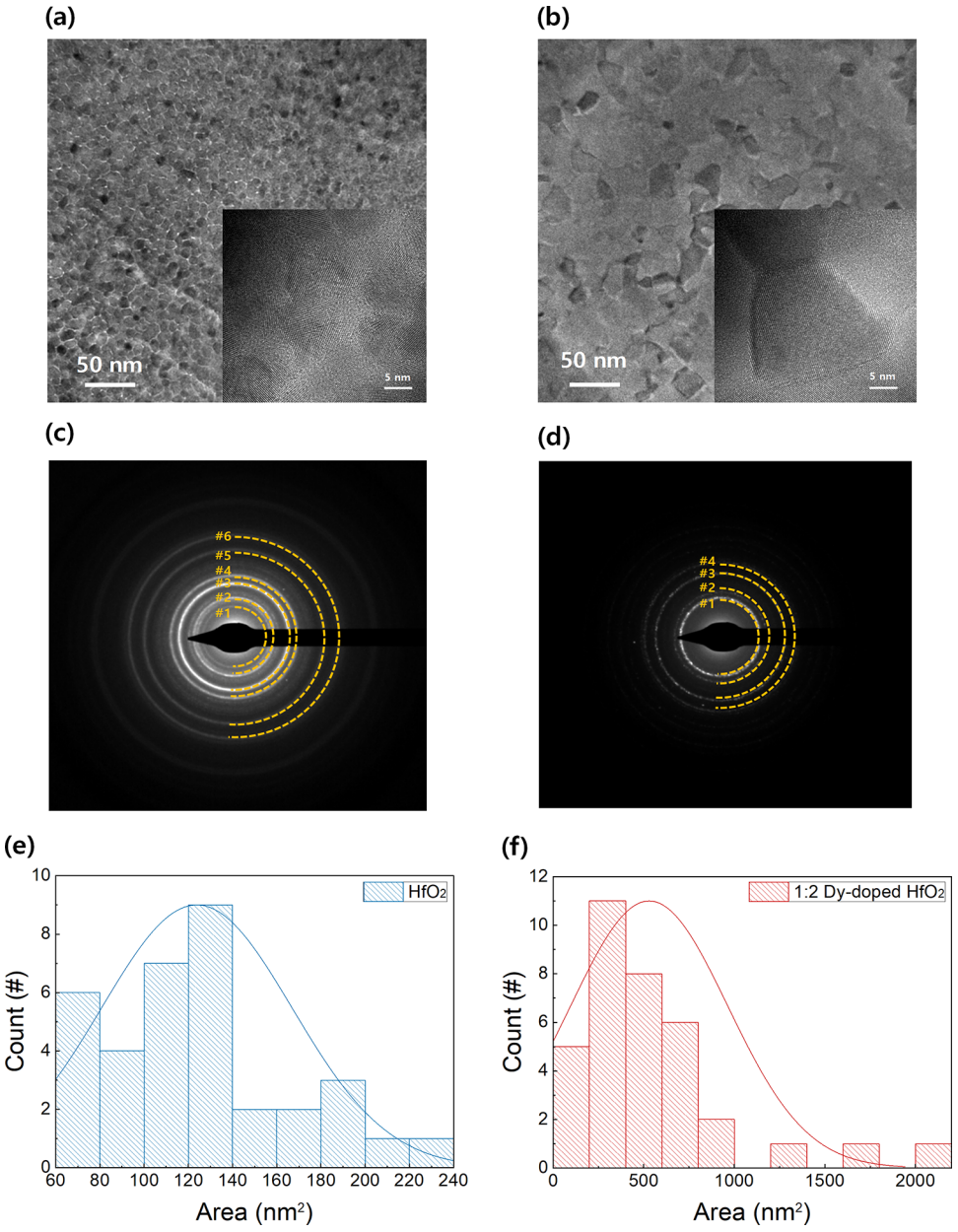

Figure 4. Plan-view TEM images of the (a) single HfO_2 film and (b) 1:2 Dy-doped HfO_2 film. SAED patterns of the (c) single HfO_2 and (d) 1:2 Dy-doped HfO_2 films. Grain size distribution histogram of the (e) single HfO_2 and (f) 1:2 Dy-doped HfO_2 films.

Figure 4c,d shows selected area diffraction (SAED) patterns of the single HfO_2 and 1:2 Dy-doped HfO_2, which were obtained from the plan-view images in Figures 4a and 4b, respectively. The SAED patterns confirm the polycrystalline nature with bright concentric rings, and the intensity of the ring patterns indicated the number of crystalline plane directions in the films. The grain size of the 1:2 Dy-doped HfO_2 films was increased compared with that of the single HfO_2 films as it was observed that the ring pattern was closer to the spots rather than the line in the same field of view. The higher intensities corresponded to the main reflection in plane (-111) of monoclinic HfO_2 indicated by #1 in Figure 4d and can be attributed to the results of preferred orientation as described in Figures 2 and 3. Table 1 shows the results of analyzing the crystallinity of single HfO_2 and 1:2 Dy-doped HfO_2 films using XRD and TEM. Various orientations present in the single HfO_2 film were transformed into the main reflection plane (-111) of monoclinic HfO_2 after Dy doping. Furthermore, Figure 4e,f depicts a histogram for the statistical comparison between the average grain sizes of both films. These are summarized in Table 2. The Dy-doped HfO_2 film had significantly larger grains in comparison with that of the HfO_2 film, which represented the reduction in the grain boundary density. In general, the grain boundary is considered as a main leakage path that can trigger degradation of the device performance. Therefore, it is envisaged that improved crystallinity of Dy-doped HfO_2 films can effectively reduce such leakage paths.

MOS capacitors structured with Ru/10 nm thick HfO_2, Dy_2O_3, and Dy-doped HfO_2 with different Dy contents/*p*-Si were fabricated to evaluate the dielectric properties of Dy-doped HfO_2 films. The *I*−*V* characteristics of the MOS samples are shown in Figure 5a. The overall leakage current densities of the Dy-doped HfO_2 samples were suppressed

https://doi.org/10.1021/acs.chemmater.2c02862
Chem. Mater. 2023, 35, 2312−2320

Table 1. Crystallinity of the Single HfO_2 and 1:2 Dy-Doped HfO_2 Films Using XRD and TEM

		XRD	SAED
HfO_2	major	m(110)	
		m(−111)	m(−111)
		m(111)	m(111)
		m(002)	
		m(−120)	m(−120)
	minor	m(120)	
		m(−211)	m(−211)
		m(112)	
		m(−112)	m(−112)
1:2 Dy-doped HfO_2	major	m(−111)	m(−111)
	minor	m(020)	
		m(−102)	m(−102)
		m(−211)	m(−211)
		m(112)	
		m(−112)	

compared with that of the HfO_2 and Dy_2O_3 samples. Figure 5b represents the leakage current values obtained at V_{FB} − 1 V/cm, which reveal the reduction by two orders of magnitude regardless of the Dy composition. The tendency of leakage current with respect to physical thickness and dielectric constant was further evaluated. Figure 5c shows the leakage current density (J_g) vs equivalent oxide thickness (EOT) plots for MOS capacitors with thickness in the range of 3−10 nm for ALD HfO_2, Dy_2O_3, and Dy-doped HfO_2 films, wherein the J_g values were measured at V_{FB} − 1 V. Dy-doped HfO_2 films exhibited significantly smaller leakage currents regardless of their thickness in comparison with that of single HfO_2 and Dy_2O_3 films. The leakage current density in gate dielectrics can be affected by various factors, such as trapped charge, band structure, film crystallinity, and film density. In the case of the trapped charge, according to a previous report, the addition of a trivalent ion dopant with a lower electronegativity than that of the host material effectively reduces the leakage current.[36] Accordingly, the Dy^{3+} ion dopant with relatively low electron negativity (1.22) stabilized the oxidation state of the host material Hf^{4+} (1.3). Therefore, it is evident that an increase in the Dy content in HfO_2 can minimize the incorporation of oxygen vacancies, thereby suppressing the contribution of hopping-type conduction in the leakage current. Additionally, defects including impurities in the thin film mainly cause the trapped charge. However, as can be seen from the RBS results (Figure 1b), the amount of impurities in the thin film was not significant. Furthermore, since small amounts of impurities can affect electrical properties, the C−V characteristics were observed as shown in Figure S2 and Table S2, but the hysteresis related to the trapped oxide charges and the interface trap density (D_{it}) values do not significantly change with Dy doping. To analyze the change in the band structure, PES measurements of single HfO_2 and Dy-doped HfO_2 films with various Dy contents were performed as shown in Figure S1 and Table S1. According to the analysis based on PES, it was assumed that Dy doping increased the conduction band offset. This decreased the electron injection from the Ru top electrode and reduced the leakage current in combination with the areal reduction of the grain boundary.

Finally, Figure 5d shows the intrinsic dielectric breakdown field (V_{BD}) of the MOS capacitors with ALD HfO_2, Dy_2O_3, and various Dy-doped HfO_2 films. It was observed that the V_{BD} characteristics were enhanced with an increase in the Dy content in the HfO_2 films compared with that of the single HfO_2 and Dy_2O_3 films, which was consistent with that of the results obtained for the leakage current. Defects such as electron traps and interface states can gradually build up in the oxide region when the electrons pass through the gate dielectric, which is indicative of the formation of the percolation leakage path between the gate and the substrate.[20] Highly energetic electrons can be generated beyond the critical electric fields due to the tremendous heat generated around these leakage paths, which facilitate the flow of current through the trap-induced paths formed in limited oxide regions. These dielectric properties can be understood using the correlation with microstructures because the density of grain boundaries significantly affects the dielectric reliability and degradation of the leakage currents. The grain boundaries function as a sink for oxygen vacancies, which incur trap-assisted tunneling currents. Hence, the generation of resulting percolation paths by randomly distributed oxygen vacancies can be preferentially located along the grain boundaries.[37] It was observed that the Dy doping led to the predominant formation of the well-aligned (−111) monoclinic phase with a large grain size, which would suppress the formation of the grain boundary density. This can explain the enhanced V_{BD} reliability and reduced leakage currents flowing through the gate stack. We also measured the film density according to the Dy doping concentration (Figure S3), but the film density slightly decreased as the Dy doping concentration increased. It is presumed that the film density of Dy-doped HfO_2 decreased as the relatively low-density Dy_2O_3 thin film was gradually incorporated. However, we observed the increased film density for 1:16 samples, which could be attributed to phase stabilization by reduced grain boundaries. Therefore, we conclude that the decrease in the number of grain boundaries and the increased conduction band offset would be predominantly responsible for the reduced leakage current density by Dy incorporation.

Additionally, recent studies have demonstrated that V_{th} modulation using a bilayer metal gate in the MOS transistor is difficult. Although V_{th} tuning can be performed by changing the metal gate work function, the magnitude of modulation has insufficient width.[38,39] To observe this, we analyzed C−V characteristics as shown in Figure S2. Electrical parameters are extracted, such as the dielectric constant, ΔV_{FB}, interface trap density (D_{it}), and hysteresis, from the C−V graphs, as summarized in Table S2. The change in V_{FB} with various Dy contents is observed and can be used for V_{th} engineering. The dielectric constant tends to decrease as the Dy doping concentration increases, consistent with our previous report.[40] Therefore, rare-earth metal (REM) doping into high-k

Table 2. Calculated Values from the Grain Size Distribution Histogram of the Single HfO_2 and 1:2 Dy-Doped HfO_2 Film

	N total	mean (nm^2)	standard deviation (nm^2)	sum (nm^2)	minimum (nm^2)	median (nm^2)	maximum (nm^2)
HfO_2	35	123.8	43.2	4334.4	66.4	121.7	230.6
1:2 Dy-doped HfO_2	35	529.7	434.2	18541.2	69.1	439.0	2041.2

https://doi.org/10.1021/acs.chemmater.2c02862
Chem. Mater. 2023, 35, 2312−2320

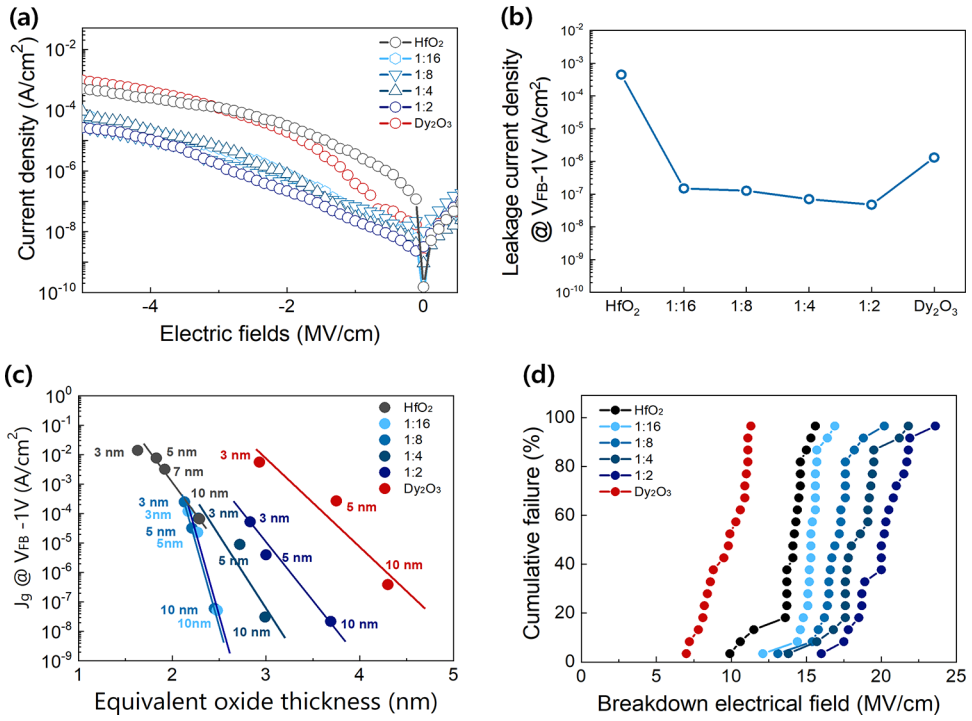

Figure 5. (a) $I-V$ curve, (b) leakage current density at $V_{FB} - 1$ V/cm, (c) leakage current density (J_g) vs equivalent oxide thickness (EOT), and (d) dielectric breakdown field (V_{BD}) of MOS capacitors with the single HfO_2, Dy_2O_3, and various Dy-doped HfO_2 films.

dielectrics can be an effective solution to modulate V_{th} compared with that of seeking a band-edge metal work function solution.[41,42]

4. CONCLUSIONS

In this study, PE-ALD Dy-doped HfO_2 films were systematically investigated, and their crystallographic properties were analyzed with respect to Dy contents controlled by ALD cycle ratio (Dy_2O_3/HfO_2). Dy incorporation enabled the phase transformation of HfO_2 films from m(110), m(−111), m(111), m(020), and m(120) to a main peak of m(−111), which indicated that Dy played a role for the phase stabilization of HfO_2 films. Furthermore, the grain size was increased by approximately 4 times due to Dy incorporation compared with that of single HfO_2, which resulted in a significant improvement in the electrical property in leakage current densities. This improvement was due to the suppression of the grain boundary formation and increased conduction band offset of Dy-doped HfO_2. A minimum leakage current density of 2.2×10^{-8} A/cm^2 (−1 MV/cm) was obtained under the experimental conditions. The Dy-doped HfO_2 films are suitable for further leakage reduction, which is an essential characteristic of high-performance and low-power devices.

■ ASSOCIATED CONTENT

Supporting Information

The Supporting Information is available free of charge at https://pubs.acs.org/doi/10.1021/acs.chemmater.2c02862.

(Figure S1) Valence band spectrum, (Table S1) $E_F - V_{BM}$, $C-V$ curve, dielectric constant, (Figure S2) flat band voltage, (Table S2) summary of the electrical properties, and (Figure S3) film density of the single HfO_2, Dy_2O_3, and Dy-doped HfO_2 films (PDF)

■ AUTHOR INFORMATION

Corresponding Authors

Woo-Hee Kim − *Department of Materials Science and Chemical Engineering, BK21 FOUR ERICA-ACE Center, Hanyang University, Ansan-si, Gyeonggi-do 15588, Korea;* orcid.org/0000-0003-0868-7479; Email: wooheekim@hanyang.ac.kr

Il-Kwon Oh − *Department of Electrical and Computer Engineering, Ajou University, Suwon 16499, Korea; Department of Intelligence Semiconductor Engineering, Ajou University, Suwon 16449, Korea;* orcid.org/0000-0002-1266-3157; Email: ikoh@ajou.ac.kr

Hyungjun Kim − *School of Electrical and Electronic Engineering, Yonsei University, Seoul 03722, Korea;* orcid.org/0000-0001-5393-2053; Email: hyungjun@yonsei.ac.kr

Authors

Yujin Lee − *School of Electrical and Electronic Engineering, Yonsei University, Seoul 03722, Korea; Department of Chemical Engineering, Stanford University, Stanford, California 94305, United States;* orcid.org/0000-0002-9213-019X

Kangsik Kim − *Center for Multidimensional Carbon Materials, Institute for Basic Science (IBS), Ulsan 44919, Korea*

Zonghoon Lee − *Center for Multidimensional Carbon Materials, Institute for Basic Science (IBS), Ulsan 44919, Korea; Department of Materials Science and Engineering, Ulsan National Institute of Science and Technology (UNIST), Ulsan 44919, Korea;* orcid.org/0000-0003-3246-4072

Hong-Sub Lee − *Department of Advanced Materials Engineering for Information and Electronics, Kyung Hee*

https://doi.org/10.1021/acs.chemmater.2c02862
Chem. Mater. 2023, 35, 2312−2320

University, Yongin, Gyeonggi-do 17104, Korea; orcid.org/0000-0001-9605-8984

Han-Bo-Ram Lee − *Department of Materials Science and Engineering, Incheon National University, Incheon 22012, Korea*

Complete contact information is available at: https://pubs.acs.org/10.1021/acs.chemmater.2c02862

Author Contributions

W.-H.K., I.-K.O., and H.K. conceived the project and designed the experiments. Y.L. and K.K. contributed equally to this work. Y.L. and K.K. conducted the experiments, performed the data analysis, conceptualized the study, prepared the manuscript, and discussed the results with all authors. Z.L., H.-S.L., and H.B.R.L. conducted the characterizations and the data analysis. All authors contributed to the manuscript.

Notes

The authors declare no competing financial interest.

■ ACKNOWLEDGMENTS

This work was conducted by the research grants (NRF-2021R1A4A1033155, NRF-2020M3F3A2A01082593, NRF-2022R1A2C2006764, NRF-2021M3H4A6A01048300, and NRF-2022R1A2C2009941) from the National Research Foundation (NRF) funded by the Ministry of Science and ICT, Korea. This work was also supported by the Technology Innovation Program (or Industrial Strategic Technology Development Program, Development of material parts package type technology) (20017392, Development of high-performance LMFC for next-generation semiconductor manufacturing, 00143986, Equipment Development for SiN Deposition with Plasma Source for MTJ Capping Layer, 20012460, Research support group for localization of ALD precursor and parts for 10 nm class semiconductor devices, and 10080527, Development of commercialization technology of highly sensitive gas sensors based on chalcogenide 2D nanomaterials) funded By the Ministry of Trade, Industry & Energy (MOTIE, Korea). This work was also supported by the Institute for Basic Science (IBS-R091-G1)

■ REFERENCES

(1) Robertson, J. High Dielectric Constant Gate Oxides for Metal Oxide Si Transistors. *Rep. Prog. Phys.* **2006**, *69*, 327−396.
(2) Houssa, M.; Pantisano, L.; Ragnarsson, L. Å.; Degraeve, R.; Schram, T.; Pourtois, G.; de Gendt, S.; Groeseneken, G.; Heyns, M. M. Electrical Properties of High-κ Gate Dielectrics: Challenges, Current Issues, and Possible Solutions. *Mater. Sci. Eng., R* **2006**, 37−85.
(3) He, G.; Zhu, L.; Sun, Z.; Wan, Q.; Zhang, L. Integrations and Challenges of Novel High-k Gate Stacks in Advanced CMOS Technology. *Prog. Mater. Sci.* **2011**, 475−572.
(4) Zhao, Y. Design of Higher-k and More Stable Rare Earth Oxides as Gate Dielectrics for Advanced CMOS Devices. *Materials* **2012**, *5*, 1413−1438.
(5) Lee, T.; Banerjee, S. K. Reduced Gate-Leakage Current and Charge Trapping Characteristics of Dysprosium-Incorporated HfO2 Gate-Oxide n-MOS Devices. *IEEE Trans. Electron Devices* **2011**, *58*, 562−566.
(6) Ando, T. Ultimate Scaling of High-κ Gate Dielectrics: Higher-κ or Interfacial Layer Scavenging? *Materials* **2012**, *5*, 478−500.
(7) Lee, H.; Jeon, S.; Hwang, H. Electrical Characteristics of a Dy-Doped HfO2 Gate Dielectric. *Appl. Phys. Lett.* **2001**, *79*, 2615.
(8) Wilk, G. D.; Wallace, R. M.; Anthony, J. M. Hafnium and Zirconium Silicates for Advanced Gate Dielectrics. *J. Appl. Phys.* **2000**, *87*, 484−492.
(9) Kingon, A. I.; Maria, J.-P.; Streiffer, S. K. Alternative Dielectrics to Silicon Dioxide for Memory and Logic Devices. *Nature* **2000**, *406*, 1032−1038.
(10) Robertson, J. Interfaces and Defects of High-K Oxides on Silicon. *Solid-State Electron.* **2005**, 283−293.
(11) George, S. M. Atomic Layer Deposition: An Overview. *Chem. Rev.* **2010**, *110*, 111−131.
(12) Mahata, C.; Byun, Y. C.; An, C. H.; Choi, S.; An, Y.; Kim, H. Comparative Study of Atomic-Layer-Deposited Stacked (HfO 2/Al2O3) and Nanolaminated (HfAlOx) Dielectrics on In0.53-Ga0.47As. *ACS Appl. Mater. Interfaces* **2013**, *5*, 4195−4201.
(13) Zhu, W. J.; Tamagawa, T.; Gibson, M.; Furukawa, T.; Ma, T. P. Effect of Al Inclusion in HfO2 on the Physical and Electrical Properties of the Dielectrics. *IEEE Electron Device Lett.* **2002**, *23*, 649−651.
(14) Visokay, M. R.; Chambers, J. J.; Rotondaro, A. L. P.; Shanware, A.; Colombo, L. Application of HfSiON as a Gate Dielectric Material. *Appl. Phys. Lett.* **2002**, *80*, 3183−3185.
(15) Yu, X.; Zhu, C.; Li, M. F.; Chin, A.; Du, A. Y.; Wang, W. D.; Kwong, D.-L. Electrical Characteristics and Suppressed Boron Penetration Behavior of Thermally Stable HfTaO Gate Dielectrics with Polycrystalline-Silicon Gate. *Appl. Phys. Lett.* **2004**, *85*, 2893−2895.
(16) Yamamoto, Y.; Kita, K.; Kyuno, K.; Toriumi, A. Structural and Electrical Properties of HfLaOx Films for an Amorphous High-k Gate Insulator. *Appl. Phys. Lett.* **2006**, *89*, No. 032903.
(17) Toriumi, A.; Kita, K.; Tomida, K.; Zhao, Y.; Widiez, J.; Nabatame, T.; Ota, H.; Hirose, M. Materials Science-Based Device Performance Engineering for Metal Gate High-k CMOS. In *IEEE International Electron Devices Meeting*; IEEE 2007; pp. 53−56. DOI: 10.1109/IEDM.2007.4418861.
(18) Jeon, S.; Hwang, H. Effect of Hygroscopic Nature on the Electrical Characteristics of Lanthanide Oxides (Pr2O3, Sm2O3, Gd2O3, and Dy2O3). *J. Appl. Phys.* **2003**, *93*, 6393−6395.
(19) Lee, T.; Choi, K.; Ando, T.; Park, D.-G.; Gribelyuk, M. A.; Kwon, U.; Banerjee, S. K. Mechanism of VFB/VTH Shift in Dysprosium Incorporated HfO2 Gate Dielectric n-Type Metal-Oxide-Semiconductor Devices. *J. Vac. Sci. Technol., B* **2011**, *29*, No. 021209.
(20) van Dover, R. B. Amorphous Lanthanide-Doped TiOx Dielectric Films. *Appl. Phys. Lett.* **1999**, *74*, 3041−3043.
(21) Park, S. J.; Kim, W. H.; Lee, H.-B.-R.; Maeng, W. J.; Kim, H. Thermal and Plasma Enhanced Atomic Layer Deposition Ruthenium and Electrical Characterization as a Metal Electrode. *Microelectron. Eng.* **2008**, *85*, 39−44.
(22) Kim, W.-H.; Kim, M.-K.; Maeng, W. J.; Gatineau, J.; Pallem, V.; Dussarrat, C.; Noori, A.; Thompson, D.; Chu, S.; Kim, H. Growth Characteristics and Film Properties of Cerium Dioxide Prepared by Plasma-Enhanced Atomic Layer Deposition. *J. Electrochem. Soc.* **2011**, *158*, G169−G172.
(23) Kim, W.-H.; Maeng, W. J.; Kim, M.-K.; Gatineau, J.; Kim, H. Electronic Structure of Cerium Oxide Gate Dielectric Grown by Plasma-Enhanced Atomic Layer Deposition. *J. Electrochem. Soc.* **2011**, *158*, G217.
(24) Oh, I. K.; Park, B. E.; Seo, S.; Yeo, B. C.; Tanskanen, J.; Lee, H. B. R.; Kim, W. H.; Kim, H. Comparative Study of the Growth Characteristics and Electrical Properties of Atomic-Layer-Deposited HfO2 Films Obtained from Metal Halide and Amide Precursors. *J. Mater. Chem. C* **2018**, *6*, 7367−7376.
(25) Oh, I. K.; Kim, K.; Lee, Z.; Ko, K. Y.; Lee, C. W.; Lee, S. J.; Myung, J. M.; Lansalot-Matras, C.; Noh, W.; Dussarrat, C.; Kim, H.; Lee, H. B. R. Hydrophobicity of Rare Earth Oxides Grown by Atomic Layer Deposition. *Chem. Mater.* **2015**, *27*, 148−156.
(26) Huang, J.; Ran, G.; Lin, J.; Shen, Q.; Lei, P.; Wang, X.; Li, N. Microstructural Evolution of Dy2O3-TiO2 Powder Mixtures during Ball Milling and Post-Milled Annealing. *Materials* **2017**, *10*, 19.

(27) Ramadoss, A.; Krishnamoorthy, K.; Kim, S. J. Novel Synthesis of Hafnium Oxide Nanoparticles by Precipitation Method and Its Characterization. *Mater. Res. Bull.* **2012**, *47*, 2680−2684.
(28) Ramana, C. V.; Bharathi, K. K.; Garcia, A.; Campbell, A. L. Growth Behavior, Lattice Expansion, Strain, and Surface Morphology of Nanocrystalline, Monoclinic HfO2 Thin Films. *J. Phys. Chem. C* **2012**, *116*, 9955−9960.
(29) Cisneros-Morales, M. C.; Aita, C. R. The Effect of Nanocrystallite Size in Monoclinic HfO2 Films on Lattice Expansion and Near-Edge Optical Absorption. *Appl. Phys. Lett.* **2010**, *96*, 191904.
(30) Shrama, S. K.; Saurakhiya, N.; Barthwal, S.; Kumar, R.; Sharma, A. Tuning of Structural, Optical, and Magnetic Properties of Ultrathin and Thin ZnO Nanowire Arrays for Nano Device Applications. *Nanoscale Res. Lett.* **2014**, *9*, 122.
(31) Sooraj, S.; Muthaiah, V. M. S.; Kang, P. C.; Koch, C. C.; Mula, S. Microstructural Evolution and Thermal Stability of Fe−Zr Metastable Alloys Developed by Mechanical Alloying Followed by Annealing. *Philos. Mag.* **2016**, *96*, 2649−2670.
(32) Khachatryan, H.; Lee, S.-N.; Kim, K.-B.; Kim, M. Deposition of Al Thin Film on Steel Substrate: The Role of Thickness on Crystallization and Grain Growth. *Metals (Basel)* **2019**, *9*, 12.
(33) Zhang, X. Y.; Hsu, C. H.; Lien, S. Y.; Wu, W. Y.; Ou, S. L.; Chen, S. Y.; Huang, W.; Zhu, W. Z.; Xiong, F. B.; Zhang, S. Temperature-Dependent HfO2/Si Interface Structural Evolution and Its Mechanism. *Nanoscale Res. Lett.* **2019**, *14*, 1−8.
(34) Biswas, D.; Singh, M. N.; Sinha, A. K.; Bhattacharyya, S.; Chakraborty, S. Effect of Excess Hafnium on HfO2 Crystallization Temperature and Leakage Current Behavior of HfO2/Si Metal-Oxide-Semiconductor Devices. *J. Vac. Sci. Technol., B: Nanotechnol. Microelectron.: Mater., Process., Meas., Phenom.* **2016**, *34*, No. 022201.
(35) Triloki; Garg, P.; Rai, R.; Singh, B. K. Structural Characterization of As-Deposited Cesium Iodide Films Studied by X-Ray Diffraction and Transmission Electron Microscopy Techniques. *Nucl. Instrum. Methods Phys. Res., Sect. A* **2014**, 128.
(36) Maeng, W. J.; Kim, W. H.; Kim, H. Flat Band Voltage (VFB) Modulation by Controlling Compositional Depth Profile in La2O3/HfO2 Nanolaminate Gate Oxide. *J. Appl. Phys.* **2010**, *107*, No. 074109.
(37) McKenna, K.; Shluger, A.; Iglesias, V.; Porti, M.; Nafráa, M.; Lanza, M.; Bersuker, G. Grain Boundary Mediated Leakage Current in Polycrystalline HfO2 Films. *Microelectron. Eng.* **2011**, *88*, 1272−1275.
(38) Lu, C. H.; Wong, G. M. T.; Birringer, R.; Dauskardt, R.; Deal, M. D.; Clemens, B. M.; Nishi, Y. Bilayer Metal Gate Electrodes with Tunable Work Function: Mechanism and Proposed Model. *J. Appl. Phys.* **2010**, *107*, No. 063710.
(39) Han, K.; Ma, X.; Yang, H.; Wang, W. Modulation of the Effective Work Function of TiN Metal Gate for PMOS Application. *J. Semicond.* **2013**, *34*, No. 086002.
(40) Park, B. E.; Lee, Y.; Oh, I. K.; Noh, W.; Gatineau, S.; Kim, H. Structural and Electrical Properties of Ge-Doped ZrO2 Thin Films Grown by Atomic Layer Deposition for High-k Dielectrics. *J. Mater. Sci.* **2018**, *53*, 15237−15245.
(41) Yamamoto, Y.; Kita, K.; Kyuno, K.; Toriumi, A. Study of La-Induced Flat Band Voltage Shift in Metal/HfLaOx/SiO2/Si Capacitors. *Jpn. J. Appl. Phys.* **2007**, *46*, 7251−7255.
(42) Wang, X. P.; Li, M.-F.; Ren, C.; Yu, X. F.; Shen, C.; Ma, H. H.; Chin, A.; Zhu, C. X.; Ning, J.; Yu, M. B.; Kwong, D. L. Tuning Effective Metal Gate Work Function by a Novel Gate Dielectric HfLaO for NMOSFETs. *IEEE Electron Device Lett.* **2006**, *27*, 31−33.

https://doi.org/10.1021/acs.chemmater.2c02862
Chem. Mater. 2023, 35, 2312−2320